7

Organic–Inorganic Mesoporous Silica Nanotube Hybrid Anodic Alumina Membranes for Ultrafine Filtration of Noble Metal Nanoparticles

Sherif A. El–Safty[1,2] and Nguyen Duc Hoa[1]
[1]*Materials Research Laboratory for Environmental and Energy*
National Institute for Materials Science (NIMS), Tsukuba-shi Ibaraki
[2]*Graduate School for Advanced Science and Engineering*
Waseda University, Shinjuku-ku, Tokyo
Japan

1. Introduction

Novel metal nanoparticles (NPs), such as gold (Au), platinum (Pt), palladium (Pd), and silver (Ag) have gained increased attention due to their distinctive physical and chemical properties as well as effective applications in catalysis, imaging, gene expression, chemical sensing, biolabeling, disease diagnostics, disease therapeutics, nanoscale electronics, and photonics. The physical and chemical properties as well as potential applications of these NPs are strongly dependent on their shapes, sizes, and structural geometries. However, conventional synthesis methods produce novel metal NPs with broad size distributions and uncontrollable precise morphologies. Therefore, it is necessary to develop a simple, effective, and fast method for separating NPs with different sizes and shapes.

Engineered control over one–dimensional (1D) mesoporous materials inside an anodic alumina membrane (AAM) has led to widespread advances in the separation of biomolecules or NPs. However, several challenges remain, particularly in applying AAM as robust nanofilters for the separation of high concentration NPs. With the aim of controlling the design functionality of nanofilters for size–exclusion cut–off separation, this book chapter focuses on the successful, up–to–date development of mesofilter designs as promising filter candidates for size–exclusive separation of NPs, in which multifunctional surface coating of the pore channels of the AAM with organic coupling agents facilitated the production of extremely robust constructed membrane sequences without the formation of air gaps among NTs. This practical nanofilter design shows evidence of controlled assessment processes that involve the evaluation of intrinsic filter properties (e.g., long–term stability, separation efficiency, and reusability, among others).

This chapter is designed to include night parts. After the introduction, an overview of the recent synthesis and characteristics of noble metal NPs (i.e., Ag, Au, Pt, and Pd) are provided. The advantages and disadvantages of conventional synthesis methods are also presented. In the third part, the basic concept of membrane separation, including filtration and nanofiltration technology, is briefly introduced. Different nanofiltration methods and their applications for small molecules, biomolecules, and NPs are discussed. In the fourth

part, the design of the high–ordered mesoporous (HOM) silica NT membrane for nanofiltration is introduced, followed by a discussion of the advantages and disadvantages of this nanofiltration process compared with other traditional methods. In the fifth part, more details about the synthesis of the high–ordered mesoporous silica membrane fabricated inside the pore channels of AAM using different surfactants are presented. We targeted the important development of mesofilter membranes composed of mesoporous silica NTs (i.e., those that are perpendicular to the longitudinal axis of the nanochannels) and uniform multidirectional pores in nanoscale sizes that effectively enhance the size–based separation of noble metal NPs within seconds. In the sixth part, the characteristics of the fabricated HOM silica NT membrane are reported. In the seventh part, the application of synthesized silica NT membranes for noble metal NPs separation is introduced. Some segments of parts of seven and eight introduce the application of high–ordered mesoporous silica NT membrane for separating novel metal NPs and their performances. Finally, the conclusion and outlook are discussed in the last part.

2. Noble metal NPs

2.1 Gold nanoparticles

Au NPs are among the most studied noble metallic NPs due to their unique physical, chemical, and bio–compatible properties as well as their potential applications (Grzelczak et al., 2008). Au NPs have been applied in various fields, included of catalysis, imaging, gene expression, chemical sensing, biolabeling, disease diagnostics, disease therapeutics, nanoscale electronics, and photonics (Nath & Chilkoti, 2002). For instance, Au NPs can be used for molecular sensing based on either surface plasmon resonance or surface–enhanced Raman spectroscopy, in which the surface plasmon resonance wavelength of Au NPs depends on their shape, size, and the dielectric constant of the surrounding medium. Therefore, any change in the local environment of the NPs leads to variations in the surface plasmon resonance wavelength and absorption band, resulting in significant detection of molecular (Enders et al., 2011). Au NPs or colloids have been investigated since the 17th century. However, the first scientific document which reported the wet chemical synthesis of Au NPs was in 1857, when Michael Faraday prepared the Au colloids by reducing gold chloride with phosphorus in water and then investigated their optical properties (Faraday, 1857). He realized that the color of Au colloid solution was red but not the yellow of traditional bulk Au. Since then, the synthesis of Au nanostructures of different sizes and shapes has become an extensive topic. Various methods have been developed to synthesize Au NPs, including wet chemical reduction by sodium citrate, ascorbic acid, sodium boron hydride, or block–copolymers in the presence of stabilizer polymers, photoreduction, microwave–assisted method, and hydrothermal method. For instance, Polte et al. investigated the mechanism of Au NP formation in the classical citrate synthesis method (Polte et al., 2010). They prepared Au NPs by reducing tetrachloroauric acid using trisodium citrate at different temperatures and reactant concentrations. The mechanistic growth of Au NPs via classical citrate synthesis method included nucleation and aggregation as well as slow and fast growth, resulting in particle sizes of 2, 3, 5.5 and 7.7 nm, respectively. Liu et al. reported the hydrothermal synthesis of spherical single crystalline Au NPs of particle size ranging from 5 to 25 nm under a basic condition (Lui et al., 2010). Hieda et al. reported the synthesis of Au NPs using plasma in aqueous solution; they used the pulsed power supply to generate discharges for the synthesis of Au NPs with exotic shapes, such as spheres, triangles, pentagons, and hexagons

(Hieda et al., 2008). Among the developed synthetic methods, wet chemical reduction of Au salts in the presence of stabilizers and reducing agents is more general and effective for the synthesis and control of Au NPs. The well–known and effective solution pathway consist of the polyol processes that include the use of poly alcohols (i.e., those containing multiple hydroxyl groups, –OH), such as ethylene glycol, propyleneglycol, diethyleneglycol, trimethyleneglycol, and butyleneglycol as a solvent and mild reducing agent (Chen et al., 2005, Carroll et al., 2011). The polyol reduction processes can be also assisted using some bases as reducing agents, including sodium borohydride or sodium bicarbonate. In the polyol processes, the polymer stabilizers, surfactants, or capping agents like poly(vinylpyrrolidone) (PVP) are used to enhance the homogenous dispersion of NPs during synthesis. In a typical synthesis, a solid inorganic precursor of Au is suspended or dissolved in liquid polyol. The solution is then stirred and heated to a given temperature, which can reach the boiling point of the polyol, in order to reduce Au metal ions. The stabilizer, such as polymer PVP, is also used to prevent the NPs from aggregation. For instance, Kim et al. reported the synthesis of Au NPs with different morphologies using a modified polyol process with the presence of the surface–regulating polymer (PVP) (Kim F. et al., 2004). Green and O'Brien reported the one phase reduction of Au (IV) chloride by sodium borohydride in hot tri–n–octylphosphine oxide as both a reaction medium and passivating ligand. The obtained Au NPs had particles of different shapes (i.e., square, triangular, and spherical) and sizes ranging from 10 to 100 nm (Green & O'Brien, 2000). Other studies have focused on the size–controlled synthesis of gold NPs, resulting in Au nanocrystals with various sizes and shapes (Xiao et al., 2011, Walker et al., 2001). Different morphologies of Au NPs have been synthesized by different pathways, as shown in Fig. 1. However, even the produced NPs still have different sizes in the optimal synthetic conditions. Thus, controlling precise shapes and/or sizes of NPs is still a challenge. A solution may be the development of general pathways, such as membrane filtration method, for size–selective separation.

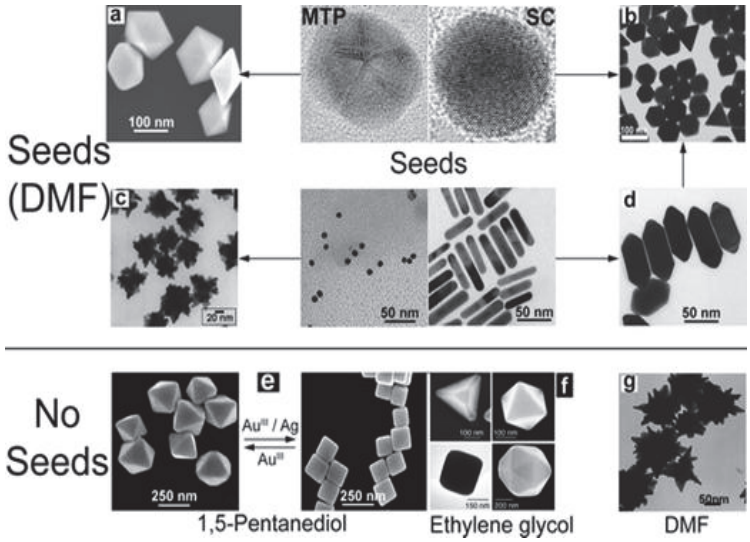

Fig. 1. TEM images of Au NPs with different shapes and sizes synthesized by different pathways (reprinted from Grzelczak et al., 2008).

2.2 Platinum nanoparticles

Recent interest on Pt materials focused on its nanostructures included of NPs, among others in order to improve their cost effectiveness and potential applications. Different morphologies of nanostructured Pt, such as nanocages, nanorods and NPs, have also been successfully fabricated (Onizawa et al., 2009, Petroski et al., 1998). The properties of Pt NPs are dependent on their shapes, sizes, and crystal structures, especially the crystallographic planes exposed on the surfaces of the NPs, thus the development of the facile method for the large–scale synthesis of Pt NPs with the ability to control the size, shape, or morphology is a crucial issue (Tsung et al., 2009). Recent research about the design of novel Pt and Pt–based nanomaterials with unique properties have been greatly intensified, because of their potential for new applications and improvement of current ones. The synthesis and control of the morphologies of Pt NPs have been extensively investigated for various applications, including catalytic applications in automobile exhaust purification, fuel–cell technology, and those for the petrochemical and fine chemical industries. To date, various methods have been developed for the synthesis of Pt NPs, including the sol−gel method, electrodeposition, electroless deposition and physical approaches, as well as the hydrothermal and solvothermal techniques (Chen A. et al., 2011). Among these, the polyol method is among the most popular pathways for synthesizing Pt NPs. This method has also been applied to synthesize metallic powders of Ru, Rh, Sn, Re, W, Pt, Au, Fe–Cu, Co–Cu, Ni–Cu, Fe, Co, Ni, Cu, Pd, and Ag (Kurihara et al., 1995, Siekkinen et al., 2006). For instance, the Xia group has introduced the process for the reduction of a Pt(II) or Pt(IV) precursor in the presence of a stabilizing polymer; the group achieved this by reducing agents, such as alcohols, sodium borohydride, or hydrogen gas (Herricks et al., 2004). In the polyol synthesis of Pt NPs, the type and amount of the surface capping–agents strongly affect the size and shape of the synthesized NPs. Polyvinylpyrrolidone is the most widely used capping agent in the synthesis of noble metal NPs. El-Sayed and coworkers controlled the shapes and sizes of the synthesis of Pt NPs by changing the concentration ratios of the capping polymer material and the platinum cations used in the reductive synthesis of colloidal particles in the solution (Ahmadi et al., 1996). The obtained products involved an abundance of different shapes, such as tetrahedal, polyhedal, irregular prismatic and cubic, and a wide particle size distribution ranging from 4 to 14 nm. Meanwhile, Miyazaki et al. synthesized the Pt NPs using polyvinylpyrrolidone, poly(N–isopropylacrylamide), and sodium polyacrylate as capping agents (Miyazaki et al., 2003). The NPs they produced had different shapes, such as hexagonal, square and triangular, depending on the capping agents used. Other methods, such as soft template (Attard et al., 1997), hard templates (Fukuoka et al., 2002) and electrochemical deposition (Tian et al., 2007), have been applied in order to control the morphologies of Pt nanocrystals. The catalytic–assisted synthesis is also an effective method for controlling the morphologies of Pt NPs. For instance, Xia and coworkers reported the synthesis of quasioctahedral shapes by simply reducing the H_2PtCl_6 precursor with PVP in aqueous solutions containing a trace amount of $FeCl_3$ (Lim et al., 2008). Another method for the synthesis of Pt NPs in an organic medium involves the Schiffrin method, in which aqueous $PtCl_6^{2-}$ ions are transferred to non–polar organic solvents by phase–transfer molecules, such as tetra–alkyl–ammonium salts reduced by borohydride treatment and capped with stabilizing alkyl isocyanide molecules (Horswell et al., 1999). The prepared particles have a well–defined crystalline structure and diameters ranging from 1 to 3 nm. Others methods, such as radiofrequency, sputtering, reverse micelles, electron beam

lithography and chemical vapor deposition techniques, have also been developed for the synthesis of Pt NPs (Welch & Compton, 2006). In general, Pt NPs can be controlled using various synthesis methods with different conditions despite the shapes and sizes; thus, the final products still produced NPs of different shapes or sizes (Fig. 2).

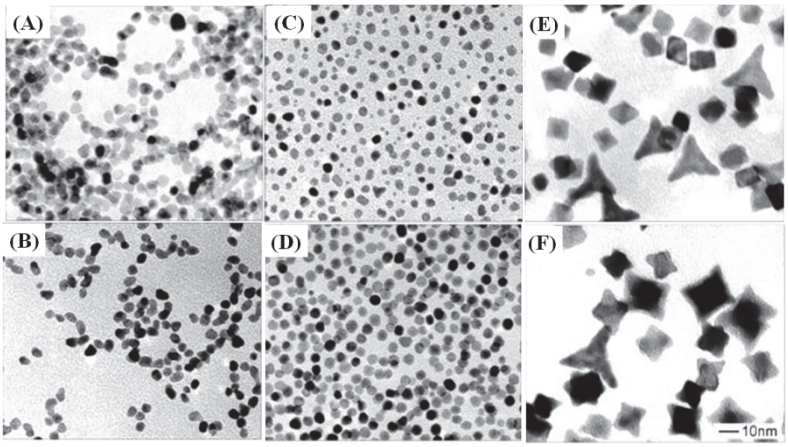

Fig. 2. TEM images of Pt NPs of different shapes and sizes (reprinted from Herricks et al., 2004)

2.3 Palladium nanoparticles

Pd is an important novel metal because of its unique physical and chemical properties and great potential applications in various fields; it can be used as a catalyst, for biological labeling, controlled drug delivery as well as electronic and optical devices (Nieto et al., 2008, Bianchini et al., 2009). However, their optical and catalytic properties and potential applications are dependent on their sizes, shapes, and morphologies. Therefore, the development of facile synthetic methods for the formation of Pd NPs with well–controlled size and shape is a very important topic that has been gaining attention in recent years (Horinouchi et al., 2006). In particular, the fabrications of noble metal NPs (including Pd) are generally conducted using wet chemical methods, such as the polyol process. A variety of Pd NPs with different shapes and sizes have been synthesized using a modified polyol reduction process in the presence of ethylene glycol and stabilizer (Xiong et al., 2005). For instance, Nemamcha et al. reported the synthesis of Pd NPs through the sonochemical reduction of Pd (II) nitrate in aqueous solution (Nemamcha et al., 2006). They prepared the starting solutions by adding different concentrations of Pd(II) nitrate in ethylene glycol and PPV. Afterwards, the resulting mixtures were irradiated with ultrasonic 50 kHz waves in a glass vessel for hours to obtain Pd NPs with particle sizes ranging from 3 to 6 nm, depending on the synthesis conditions. Roy et al. reported the characteristics of Pd NPs obtained by a one–pot reduction of Pd chloride in aqueous solution using citric acid in the presence of steric stabilizer polyvinylalcohol (Roy et al., 2006). The diameters of the Pd NPs can be controlled in a range of ~8–53 nm, using different synthesis conditions, such as reflux time, concentrations of metal ion, reducing agent, and capping polymer. The solution and seed–mediated growth methods have also been reported on the size and shape evolution of metal nanostructures. For instance, Kim et al. reported on the synthesis of monodisperse Pd

NPs by thermal decomposition of a Pd−surfactant complex (Kim SW. et al., 2003). They controlled the particle size of Pd NPs within 3.5–7 nm by varying the concentration of the stabilizing surfactant. Niu et al. introduced the shape–controlled synthesis of Pd nanocrystals via the seed–mediated method with CTAB, potassium iodide, and ascorbic acid as the surfactant additive and reductant, respectively (Niu et al., 2010). Several types of Pd nanocrystals, such as rhombic dodecahedral, cubic and octahedral have been prepared by manipulating potassium iodide concentration and the reaction temperature. However, synthesizing Pd NPs with fine and narrow particle size distribution is still a challenge. Pd NPs of different shapes and sizes fabricated by wet chemical route are shown in Fig. 3.

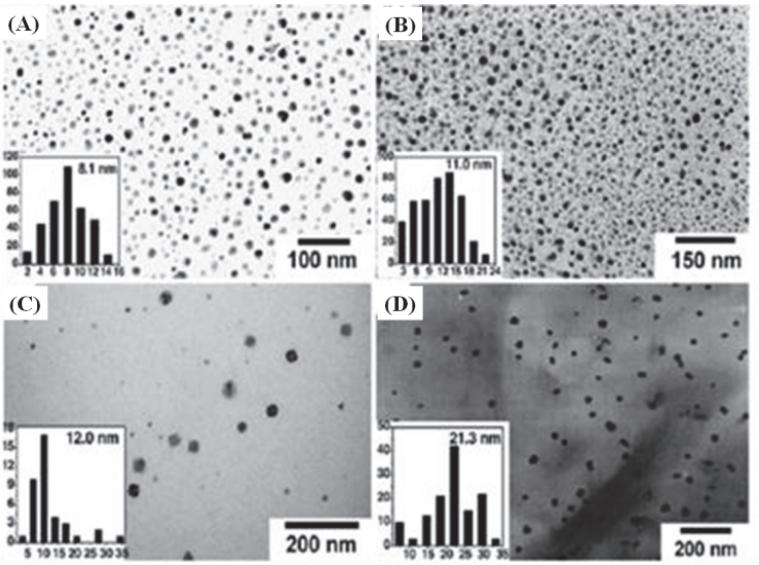

Fig. 3. TEM images and size distributions of Pd NPs of different morphologies (reprinted from Xia et al., 2009)

2.4 Silver nanoparticles

Ag NPs and their related nanostructures have been investigated extensively, because of their unique properties and great potential applications in oplasmonics, anti–bacterial materials, sensing, and spectroscopy. For instance, the anti–bacterial activity and good conductivity of Ag have been known since the ancient times and are now widely investigated for real applications (Kosmala et al., 1011). In addition, Ag NPs exhibit the surface plasmon resonance effect and strong bacterial resistance to antibiotics, making them ideal for biotechnological applications (Shrivastava et al., 2009). Ag NPs can be synthesized using various methods, such as chemical reduction (Pal et al., 2007), electrochemical (Santos et al., 2002), γ–radiation (Choi et al., 2005), laser ablation (Amendola et al., 2007), solvothermal (Yang et al., 2007), hydrothermal (Shen et al., 2011), photochemical (Henglein, 1998), and sonochemical (Salkar et al., 1999). Generally, different shapes and sizes of Ag NPs can be fabricated by wet chemical routes just simply varying the synthetic conditions. For instance, Dong et al. reported the synthesis of triangular Ag nanoprisms via stepwise

reduction of Ag nitrate with sodium borohydride and trisodium citrate (Dong et al., 2010). They realized that the formation of the triangular nanoprisms is dependent on the molar ratios of sodium borohydride and trisodium citrate used in the reactions, in which a balance between the precursor contributed to the formation of the small spherical particles. The transformation of the spherical NPs is critical for the synthesis of the triangular nanoprisms. The TEM images of obtained silver NPs are shown in Fig. 4, and as can be seen, the Ag NPs have different shapes and sizes depending on the reduction time.

In summary, almost all aforementioned methods used the reducing agents to reduce the Ag salts to form Ag NPs with different shapes and sizes by carefully controlling the reducing environment and stabilizer concentration during synthesis. However, none of the above methods appear suitable for general utility. Most methods offer an acceptably narrow size distribution; however, they do not offer much variability in the size that can be produced. The preparation of Ag NPs with homogenous particle size is highly important in increasing their potential applications.

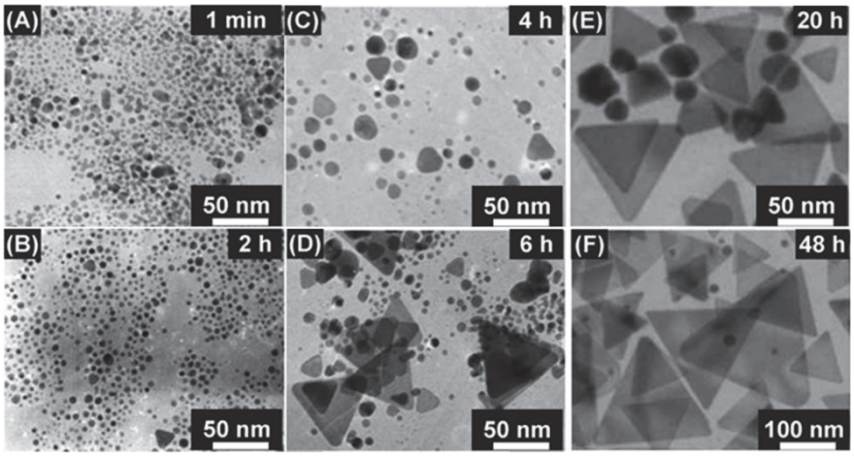

Fig. 4. TEM images of Ag NPs obtained through different time duration reductions of silver nitrate by sodium borohydride (reprinted from Dong et al., 2010)

2.5 Optical properties of novel metal NPs

Noble metal NPs exhibit diverse and unique characteristics, including catalytic, electronic, and optical properties. Among other, their optical properties are most interesting because of the interactions of electromagnetic field from the light and NPs, resulting different colors of NPs. For instant, the color of Au colloidal solution can be changed from red to light blue by varying the size and shapes of NPs (Jones et al., 2011). The abnormal behaviors have been attributed to the interaction between the electromagnetic radiation and the conduction band electrons (free electron cloud) of NPs (Fig.5).

When the oscillating electric field from incident light interacts with the delocalized electrons of a metal, the free electron cloud is perturbed and displaced from the metal framework, thus generating a dipole in the NP. However, the Coulombic attraction from the positively charged nuclei of the metal pulls the electron cloud back to its initial position. Due to the large

difference in mass, the heavy nuclei remain in a fixed position, whereas the lighter electrons experience motion. With the electric field component of incident light acting as a sinusoidal driving force and Coulombic attraction acting as a restoring force, all components of a harmonic oscillator are present. Consequently, resonant conditions can be achieved when light is coupled in phase to the natural frequency of the plasmon oscillation. At these resonant conditions, the metal structures absorb the maximum amount of incident electromagnetic radiation, thereby causing the greatest amount of charge displacement. The oscillation wavelength depends strongly on the surrounding medium, size and shape of NP, which lead to different surface plasmon bands of NP solutions and different colors, as shown in Fig. 6.

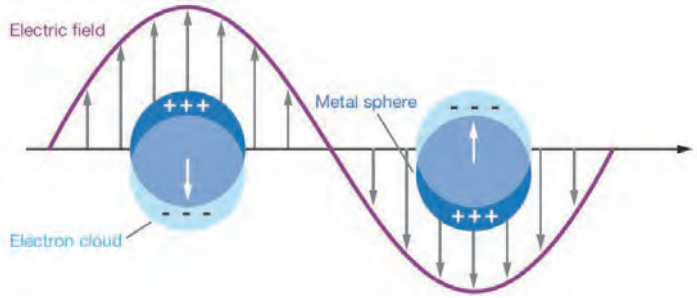

Fig. 5. Schematic diagram illustrating a localized surface plasmon (reprinted from Willets & Duyne, 2007)

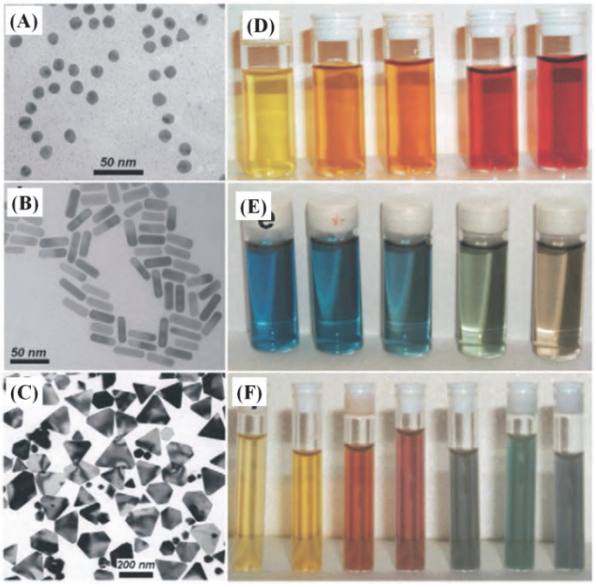

Fig. 6. Left: Transmission electron micrographs of Au nanospheres and nanorods (a,b) and Ag nanoprisms (c, mostly truncated triangles). Right: Photographs of colloidal dispersions of Au–Ag alloy NPs with increasing Au concentration (d), Au nanorods of increasing aspect ratio (e), and Ag nanoprisms with increasing lateral size (f) (reprinted from(Liz–Marzán, 2004))

3. Basic concepts of membrane separation

3.1 Overview of membrane separation

The separation of different molecules, ions, and particles from their mixture is a critical issue in the fields of nanoscience, nanotechnology, and especially in pharmacy and biology (Han et al., 2008). In recent years, several separation methods have been developed, including membrane filtration, size–exclusion chromatography, and electrophoresis. Membrane–based separations are becoming increasingly relevant for a number of applications due to their low energy requirements, potentially low fabrication cost, and steady–state operation (Jang et al., 2011). The membrane filtrations have been applied for the separation of gas phases, liquid–liquid phases, submicron particles from water, organic mixture, and hydrocabon mixture (Gin et al., 1011). They are very effective in separating molecules of different sizes, solids from liquids, and/or large size particles from small sizes by imperatively imposing the mixture solution through the proper porous membranes (Soria, 1995, Asatekin et al., 2011). Synthetic membranes have been developed and used in many separation processes, from industrial–scale ones (e.g., separating atmospheric gases for medical and industrial use and removing salt from seawater) to smaller–scale processes in chemical synthesis and purification, in which the membranes work by forming a barrier between two phases (e.g., salt water and fresh water) that restrict the movement of some molecules while allowing others to pass through. Diverse types of membrane filtration have been investigated and manufactured for the separation of gases, molecules, and particles of different sizes, permeabilities, and hydrophobicities. The membranes are classified as either dense (nonporous) or porous, depending on how the molecules (filtrates) move across the barrier. The porous membranes are further divided into asymmetric and symmetric. Those membranes have been classified based on their porous characteristics (Table 1).

Membrane barrier structure	Trans–membrane gradient		
	Concentration	Pressure	Electrical field
Non–porous Microporous dp≤2 nm Mesoporous dp=2–50 nm Macroporous dp=50–500 nm	P evaporation (PV) Dialysis (D) Dialysis	Gas separation (GS) Nanofiltration (NF) Ultrafiltration (UF) Microfiltration (MF)	Electrodialysis (ED) Electrodialysis

Table 1. Classification of membranes and membrane process for separation via passive transport (Ulbricht, 2006)

The membranes are classified as non–porous (dense), microporous (d_p≤2 nm), mesoporous (d_p=2–50 nm), and macroporous (d_p=50–500 nm) based on the barrier structure. These membranes are also classified if they are intended for gas separation (GS), reverse osmosis (RO), nano–filtration (NF), ultra–filtration (UF), and micro–filtration (MF) based on the trans–membrane gradient. The separation based on the gradient of concentration is classified into pressure evaporation and dialysis. However, the classifications are relative and associated. For instance, the pore sizes of RO, NF, UF, and MF fall within the ranges of

10^{-4}–10^{-3}, 10^{-3}–10^{-2}, 10^{-2}–10^{-1} and 10^{-1}–10^{1} μm, respectively (Wagner, 2001). The GS is used for air separation or natural gas purification, such as H_2, He, O_2, N_2, CO_2, C_2H_6, C_3H_8, and CH_4. The RO membrane is applied in liquid/liquid separation, where the water is the only material passing through the membrane. RO is effectively used to purify water, especially in successful applications for desalination of sea and brackish water, waste treatment, and various separations in chemical, food, pharmaceutical, and other industries; all dissolved and suspended material are rejected through the membrane. The NF rejects only ions with more than one negative charge, such as sulfate or phosphate, while passing single charged ions. NF also rejects uncharged, dissolved materials, and positively charged ions according to the size and shape of the molecule in question. UF is a process, in which the high molecular weight component (e.g., protein and suspended solids) are rejected, whereas all low molecular weight components pass through the membrane freely. Mono– and di–saccharides, salts, amino acids, organics, inorganicacids, or sodium hydroxide are not rejected by UF. The MF is a process where in only suspended solids are rejected, whereas proteins pass the membrane freely.

The membrane filtration can be classified as organic (e.g., polyethylene terephthalate, cellulose acetate, polyvinylidenedifluoride) and inorganic (e.g., carbon, alumina, silica) types based on the materials. In addition, they can be classified as having flat and hollow fiber forms based on the geometries. For instance, the commercial ordered porous organic polymeric membrances are track–etched polycarbonate and polyethylene terephthalate, whereas the commercial available inorganic membranes are glass, metal, zirconia, zeolite, and alumina (Robeson, 2008, Choi et al., 2009). Figure 7 shows the SEM images of hollow fiber poly(vinylidenefluoride), (a) hollow fiber carbon, (b) photos of commercial track etched polycarbonate, and the (c) high–ordered porous anodic alumina membranes (d).

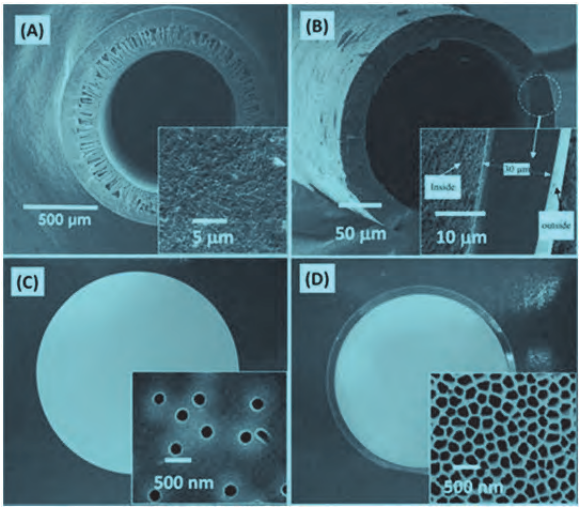

Fig. 7. The hollow fiber and flat membranes: (a) SEM images of hollow fiber poly(vinylidene fluoride) membranes (reprinted from Hashim et al., 2011); (b) Hollow fiber carbon membranes (reprinted from He at al., 2011) and photos of 47 mm diameter; (c) track–etched polycarbonate;(d) and anodic alumina membranes (insets are respective SEM images).

The membrane can be designed with the most appropriate geometry, size, and characteristics, depending on the purpose of application. Polymeric membrane filtrations are more popular than their inorganic counterparts, because they have the advantage of easy handling and better functionality (high selectivity). They are also suited for large–scale, low–cost fabrication processes, and can be designed with different structures (e.g., hollow, porous fibers or porous films). However, they suffer from several limitations such as low permeance, high temperature instability, as well as swelling and decomposition of organic solvents. On the other hand, inorganic membranes, such as porous anodic alumina, zeolite and porous silica possess high permeability, tunable selectivity, and high thermal and chemical resistance (Hsieh, 1991). The potential application of inorganic membranes is widely recognized since the production of high–quality porous ceramic membranes for large–scale industrial usage have been realized. Some inorganic membranes, such as mica, glass and alumina, are commercially available nowadays. Despite the extensive development and investigation of inorganic membranes for the separation of liquids and gases, reports on porous membranes for NP separation are rare, especially those for separating noble metals that are less than 10 nm in particle size.

3.2 Ultrafiltration and nanofiltration membranes

For the separation of NPs that are less than 10 nm in size, membranes should have proper porous structures, with a homogenous pore size distribution. Ultrafiltration and nanofiltration membranes are actually ideal candidates for separating NPs and large molecules, such as proteins, because they have pore sizes in the range of 1–100 nm. Ultrafiltration and nanofiltration membranes have been extensively used in industry and research for purifying and concentrating macromolecular solutions (Iglesias et al., 2009). They are effective in separating proteins and NPs due to the simplicity of the process and their tunable proper pore sizes. Ultrafiltration and nanofiltration membranes also enable the continuous separation of a large volume of feed, in which the feed stream is applied using a relative high pressure that forces the mixture against the porous membrane. The solutes with high molecular weight and large particles are retained, while those with low molecular weight and small particles pass through the membrane. Using ultrafiltration membranes, it is easy to separate the large and small particles as well as the large and small molecules through the size cut–off sieving processes. Polymer ultrafiltration membranes used for separation by a variety of food, biological, and pharmaceutical systems, as well as by the water purification and treatment industries, have been well–developed and are commercially available. However, polymeric membranes are not effective in separating NPs, because of their low porous density. In addition, they exhibit lower selectivity, poor thermal and chemical stability than inorganic counterparts. Inorganic membranes have high thermal chemical stabilities, and some inorganic membranes, such as glass, metal, alumina, zirconia, zeolite, and carbon membranes are commercially available. Despite that, these membranes vary greatly in pore size, support material, and configuration; in addition, they are not efficient in separating noble metal NPs. Furthermore, the design of a proper anisotropic porous inorganic membrane with higher flux, better selectivity, thermal stability, and chemical stability for the separation of large molecules and NPs remains a challenge. The fabrication design of the hierarchal mesoporous filter membranes with nano–space pores and of chemically robust and mechanically stable NTs can solve those problems.

3.3 Filtration flow methods

During membrane filtration, flow directions or filtration methods have a great impact on separation performances. Fig.8 illustrates two types of flow filtration, namely, tangential (cross) flow (A) and dead–end flow (B). In the tangential flow filtration shown in Fig. 8(A), the feed stream is applied tangential to the surface of the porous membrane (i.e., crossing the pore channels of the membrane). This feeding flow method minimizes membrane fouling, maintains a high filtration rate and ensures higher product recovery, because the sample remains safely in solution separation and the retentate stays on the surface of the membrane. To be usable for tangential flow filtration, the membranes are designed as tubular or hollow fiber membranes, as shown in Figs. 7(A)–(B). In the dead–end filtration shown in Fig. 8(B), the feed is applied perpendicularly to the surface of the membrane (i.e., feed stream flows through the pore channels of the membrane). This flow method enables rapid separation, because the feed is forced against the membrane surface. To be usable for dead–end flow filtration, the membranes are designed as flat sheets, as shown in Figs. 7(C)–(D). However, flat sheet membranes require the product stream to spread across the entire surface of the individual sheets prior to recirculation. This non–uniform flow path causes build–up and product loss in the "membrane corners" that see slower flow rates. In addition, dead–end filtration results in a build–up of product on the membrane surface; this may damage the product and cause lower recovery, thereby "fouling" the membrane.

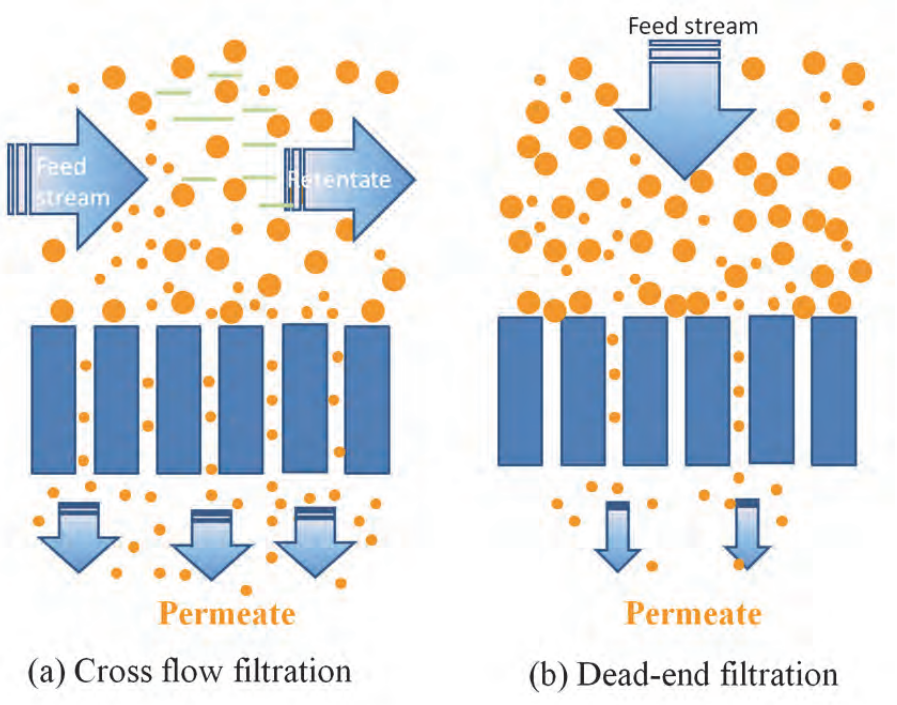

Fig. 8. Schematic diagram of (a) tangential (cross) flow filtration and (b) dead–end filtration

4. Design of HOM silica NTs membranes for nanofiltration

Silica NTs have been investigated extensively since their discovery in 1995 (Nakamura &. Matsui, 1995). Thereafter, enormous efforts have been devoted to identify their synthesis, fundamental properties, and applications. To date, researchers have been able to fabricate nanofibers, NTs, nanowires, and nanorods of high alignment and with the ability to control the porous structures by combining the use of soft and hard templates. Substantial efforts have particularly been devoted to the fabrication of 1D or two–dimensional (2D) hexagonally ordered or stacked doughnut (circular) silica mesostructures inside the columnar pores of the AAM nanochannels using template–guided syntheses. The synthesis pathway is the so–called dual template method has been widely used to fabricate a range of 1D and 2D mesostructures of silica, carbon, polymer, and metals. However, controlling the mesopore geometry and dimension into the AAM nanochannels has generally required labor–intensive or complicated design strategies that involve aging time, temperature, pH, and humidity. Table 2 provides a brief summary of the fabrication of hierarchical mesoporous structures inside the 1D nanochannels synthesized in AAM templates. A feasible control over the engineering of 2D hexagonal and 3D mesopore cubic *Im3m* cage structures in the entire silica NTs that are well–aligned with AAM nanochannels has also been recently reported (see Table 2).

In general, dual template pathways have been applied in synthesizing silica NTs of porous structures (see table 2). This synthetic pathway uses the AAM pore channels as the hard template to maintain the tubular structure of the silica, whereas the self–assembly of the liquid crystal or surfactant is used as the soft template to control the porous structure of the silica. This general synthetic pathway can be extended by varying synthetic conditions, including the composition and type of surfactants for synthesizing various mesoporous structures of silica NTs. The use of dual template for the synthesis of highly ordered mesoporous silica NTs has some advantages, including the ability to control the porous structure of silica NTs, homogenous pore size distribution, and the enhancement of the mechanical stability of membrane. However, to improve the mesoporous membranes synthesized using AAM as hard templates, the following chemical and mechanical stability problems must be addressed: (1) synthesis of robust, tubular structures into the entire AAM nanochannels; the (2) formation of unconnected pores and irregular shapes due to the detachment of mesoporous silica NTs from the AAM walls; (3) creation of air gaps within the shrinking mesoporous silica upon high–temperature calcination of soft templates; and (4) low–term chemical stability of the membrane within the separation reuse–cycles (El–Safty et al., 2010, 2011). Normally, the manufacturing defects in mesoporous silica NT hybrid AAM limit the long–term storage stability of NTs inside AAM (even for a month) and reduce the potential of NT filtration systems to control the filtration rates and diffusivity of NPs. Therefore, the fabrication design of chemically robust and mechanically stable NTs as well as hierarchal mesoporous filter membranes with nano–space pores remains a key challenge in the field of materials science.

The development of a new strategy leading to synthetically constructed mesostructures with tunable pore sizes throughout the 1D nanochannels is highly desirable for the size–exclusion separation of macromolecules and NPs. As a more detailed example, a method for the fabrication of hierarchal mesofilters based on the nanolinker approach templated inside the nanochannels of AAM has been successfully developed in recent years. In this development method, impermeable layers coated with silica NT hybrid AAM have been used to create chemically robust and mechanically stable designs, as shown in Fig. 9.

Structure types	Synthesis techniques and surfactants [a]	Properties	Application	Ref.
Mesoporous silica NFs	Vapor phase synthesis (PVS), using and F127, CTAB, DTAB, and OTAB templates	Pore size= 9 and 7 nm, S_{BET}=651 and 736 m^2g^{-1}	Catalytic Knoevenagel condensation	(Lee et al., 2009)
Mesoporous silica NFs	Sol–gel process, using P123 template	Pore size=7 nm; S_{BET} = 73.0 and 28.7m^2 g^{-1}	---[b]	(Gong et al., 2009)
Mesoporous silica NFs	Vapor–deposition hydrolysis, using OTAB, DeTAB, DTAB, TTAB, and CTAB surfactants	S_{BET} = 554, 610, and 780 m^2 g^{-1}	---[b]	(Lee et al., 2008)
Mesoporous carbon NFs	Sol–gel process, using P123 template	---	---[b]	(Cott et al., 2006)
Mesoporous silica NRs	Electrophoretic deposition, using P123 template	Pore size 10 nm	---[b]	(Hill et al., 2009)
Mesoporous silica NRs	Dip–coating method, using Brij 56 template	Pore size 4–5 nm	Gas separation	(Yoo et al., 2006)
Mesoporous silica NRs	sol–gel dip–coating method, P123 templates	---	Templates for synthesis of Ag, Ni, Cu_2O NWs	(Wu et al., 2004)
Mesoporous silica NRs	EISA method, CTAB, P123 and Brij 56	Pore size 8–9 nm; S_{BET}= 43– 55 m^2g^{-1}	---	(Platschek et al., 2008)
Mesoporous silica NRs	Sol–gel casting method, P123 template	Pore size 3–30 nm	Templates for synthesis of Cu, Ag, Te NWs	(Moses et al., 2010)
2D mesoporous silica NSs	Microemulsion liquid crystal phases of CTAB, DDAB, Brij. 30, 35, 56, 58, 76, 78, 97, 98 surfactants	S_{BET} =28.6–100 m^2g^{-1} Pore size= 3.7 – 5.1 nm	Separation of NPs	(El–Safty et al., 2010, 2011)
3D mesocage silica NTs	Microemulsion liquid crystal phases of F108, F127 surfactants	S_{BET} =100– 310 m^2/g	Separation of biomolecules	(El–Safty et al., 2010, 2011)

[a]Pluronic P123 ($EO_{20}PO_{70}EO_{20}$); Pluronic F127 ($PEO_{100}PPO_{70}PEO_{100}$), Pluronic F108 ($EO_{141}PO_{44}EO_{141}$), hexadecyltrimethylammo–niumbromide (CTAB), dilauryldimethylammonium bromide (DDAB), dodecyltrimethly–ammoniumbromide(DTAB),octyltrimethyl–ammoniumbromide(OTAB),decyltrimethyl–ammoniumbromide(DeTAB),tetradecyltrimethyl–ammoniumbromide (TTAB). [b] Not used for any applications.

Table 2. Fabrication, properties, and feasible applications of mesoporous structures inside nanowires (NWs), Nanofibers (NFs), nanorods (NRs), nanostrands (NSs), and nanotubes (NTs) hybrid AAM channels

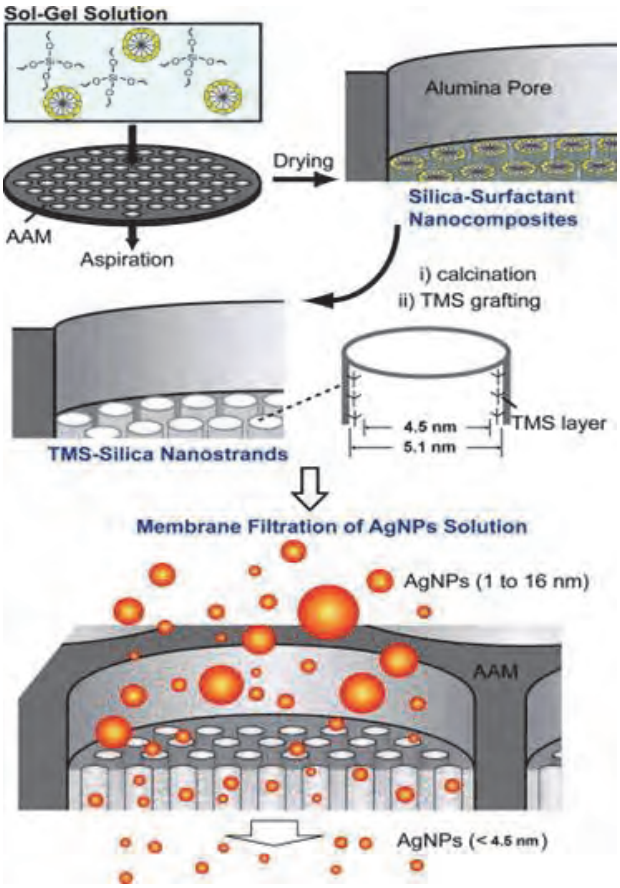

Fig. 9. Schematic design for the fabrication of mesoporous silica hybrid AAM and the size–exclusive separation system (reprinted from El–Safty et al., 2011)

The synthesis of densely–engineered mesofilters has been achieved using the following steps. First, the 2D hexagonal and 3D cubic *Im3m* mesoporous silica–NTs were synthesized inside the AAM or TMAC–AAM linkers using a direct templating method with cationic or nonionic surfactants. A key advantage of this approach is the capability to control the building of mesopores throughout the AAM nanochannels. Notably, the use of the direct templating method can lead to a more thermodynamically stable phase with hexagonal and 3D cubic *Im3m* structures inside the AAM nanolinkers. In addition, layered surface chemistry has been achieved by coating the inner mesopores inside the silica NTs with hydrophobic trimethylsilyl (TMS) groups. The hydrophobic TMS coating in mesoporous NTs can lead to the treatment of the tortuous–pore openings that form during the removal of the soft templates. In this approach, the organic monolayers (TMS) are densely packed and are highly stable under thermal conditions. This mesofilter membrane design is the key to broadening the nanofiltration applications for bio–molecule and NP separation.

5. Fabrication of HOM silica NTs using direct–templating method

The formation of hierarchically ordered silica NTs can be achieved by templating microemulsion liquid crystal phases with different surfactants inside AAM to control the mesoporous structures of the NTs. A typical synthesis of highly ordered mesoporous silica NTs on AAM templates includes the following: (i) the fabrication of a microemulsion precursor, and (ii) penetration of the microemulsion precursor in the pore channels of the AAM template, followed by (iii) calcinations at high temperature or extraction to remove the surfactants.

The schematic diagram of a system used for the synthesis of highly ordered silica NTs and the nanofiltration separation of noble metal NPs is shown in Fig. 10. When used to fabricate the HOM silica NT membrane, the pristine AAM is settled in the system, after which the precursor solution is dropped to fill in its pore channels with the assistance of slight vacuum pumping. After drying and calcinations, the HOM silica NTs were obtained inside the pore channels of AAM. However, when used for NPs separation, the HOM silica NT membrane is settled in a filtering system instead of a pristine AAM; then, the solution of NPs is dropped into the filtering funnel. Using vacuum pumping, the solution is separated through the membrane. In this regard, the NPs may go through the membrane with a smaller particle size than the pore diameter of NTs, whereas those with a larger particle size are retained in the filtering tunnel. The separated size of NPs is controlled by the pore size of silica NTs; in turn, the pore size and pore structure of silica NTs can be controlled by varying the surfactants and compositions.

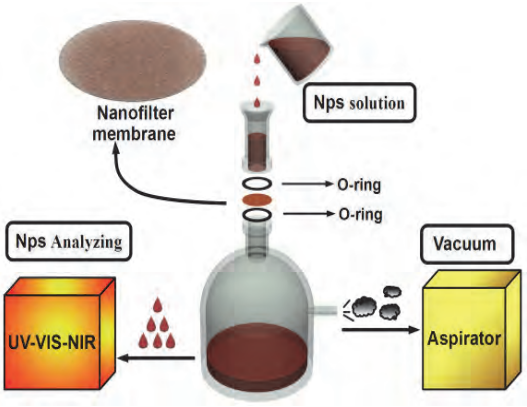

Fig. 10. Schematic diagram of a nanofiltration system used for the synthesis of highly ordered silica NT membrane and the NP filtration (El–Safty et al., 2010, 2011)

5.1 Synthesis of HOM silicas NTs using Brij–type (C_xEO_y) templates

Typically, Brij–type surfactants were dissolved in a mixture of ethanol and acidic aqueous solution (H_2O/HCl). The resultant mixture was stirred for 30 min under refluxing conditions. Then, tetraethyl orthosilicate (TEOS) was added dropwise to the mixture, with continuous stirring at 30 °C for 2.5 h. The precursor solution was added dropwise into the AAM. Moderate aspiration was applied using an aspirator (Ulvac, Model MD A–15),

leading to the penetration of the precursor solution into the columnar alumina pores. The resultant surfactant–silica hybrid membrane was then dried at room temperature for 1 h. The surfactant was removed by calcination at 600 °C for 2 h under air, using a Yamato FO 310 muffle furnace with a temperature rate of 2 °C/min (El–Safty et al., 2010).

5.2 Synthesis of HOM silica NTs using CTAB templates

Briefly, the microemulsion phase domains containing TMOS, cationic surfactants (DDAB, CTAB), decane, HCl–H_2O, and EtOH at their molar compositions of 1:0.165:2.08:8.284 and 1:0.209:2.08:8.284 for DDAB and CTAB systems, respectively, were obtained by mixing thoroughly for 30 min. The penetration of the microemulsion domains into the AAM was done by means of a gentle vacuuming pressure of ≤0.04 MPa. The silica NTs were allowed to stand in a sealed container at 45 °C for 10 h to complete the drying process. The AAM embedded microemulsion phases were calcined at 600 °C in air for 3 h to remove the organic compounds and form the mesoporous silica NTs (El–Safty et al., 2010).

5.3 Synthesis of HOM silicas NTs using F108 templates

Quaternary microemulsion liquid crystalline phases of triblock copolymer F108/C_{12}–alkane/TMOS/H_2O–HCl were used to facilitate the template–guided synthesis of 3D mesocage surfactant/silica phases inside AAM. In this direct synthesis, the precursor solution containing TMOS, F108, dodecane, H_2O–HCl, and ethanol at a respective molar composition ratio of 1:0.00732:0.313:2.59:16.56 was applied dropwise into the AAM nanochannels. Penetration of the precursor solution into the membrane was achieved by means of vacuum at a starting pressure of ≤0.04 MPa, thus allowing control of the silica–NTs inside the membrane pores. The addition of C12–alkane led to the formation of 3D cubic *Im3m* structures with large cage pores and uniform open entrances. The hybrid organic–inorganic membrane was allowed to stand in a sealed container at 45 °C for 10 h to complete the drying process. The organic moieties were removed by calcination at 600 °C under air (El–Safty et al., 2010, 2011).

5.4 Synthesis of HOM silicas NTs using F127 templates

The quaternary microemulsion liquid crystalline phases of triblock copolymer F127/C_{12}–alkane/TMOS/H_2O–HCl (1.4 g of F127, 0.7 g of dodecane, 2 g of TMOS, 1.25 g of H_2O–HCl, and 10 g of ethanol) were used to facilitate template–guided synthesis of 3D mesocage surfactant/silica phases. The precursor solution was applied dropwise into the TMAC–AAM nanochannels (TMCS=trimethylcholrosilane)). Penetration of the precursor solution into the membrane was achieved by means of vacuum at a pressure of ≤ 0.04 MPa. It is important to note that the use of the quaternary microemulsion liquid crystalline phase could lead to a more thermodynamically stable phase with a high curvature of cubic *Im3m* geometry. Furthermore, the addition of C_{12}–alkane led to the formation of 3D cubic *Im3m* structures with large cage pores and uniform open entrances. The hybrid organic–inorganic membrane was allowed to stand in a sealed container at 45 °C for 10 h to complete the drying process. Next, the hybrid organic–inorganic membrane was washed thoroughly with ethanol/acidified H_2O for several cycles in a Soxhlet apparatus to remove the F127 surfactant template; this was then dried at 60 °C.

In general, the quaternary microemulsion liquid crystalline phases of triblock copolymers were used as a template–guided synthesis of cubic *Im3m* mesocage pores inside the NTs. The 3D mesopore cubic *Im3m* cage array with uniform entrances (~5 nm) and large cavities (~17.3 nm) inside AAM allowed the development of size–exclusion nano–filter membranes (El–Safty et al., 2010, 2011).

6. Characteristics of HOM silica NTs membranes

The study of vertically–aligned nanochannels and the coexistence of circular or columnar mesopores and mesostructured geometries inside the AAM channels has gained considerable research attention in recent years. Such architectures inside the AAM channels are very effective for the size–exclusion separation of macromolecules and NPs. In this section, the characteristics of fabricated HOM silica NTs inside nanopores of AAM are investigated using various tools of analyses, such as nitrogen adsorption/desorption isotherm, small–angle X–ray scattering (SAXS), field emission scanning electron microscopy (FE–SEM), and high–resolution transmission electron microscopy (HRTEM). Details about the characterization method can be found in references (Hoa & El–Safty, 2011).

The advanced SAXS technique is one of the most powerful methods in investigating the mesoporous structure of HOM silica NTs. As reported in recent publications, silica NTs prepared using different surfactants and compositions have different mesophase structures, such as hexagonal and cubic *Im3m* or disordered mesostructures (El–Safty et al., 2010, 2011). As an example, Fig. 11 (A) shows the SAXS patterns of porous silica NTs fabricated inside the AAM pore channels using triblock copolymers of Pluronic F127 as a template. The silica NTs exhibit the cubic *Im3m* mesostructure. The inset of Fig. 11(A) is the structural parameters of fabricated HOM silica NTs characterized by SAXS.

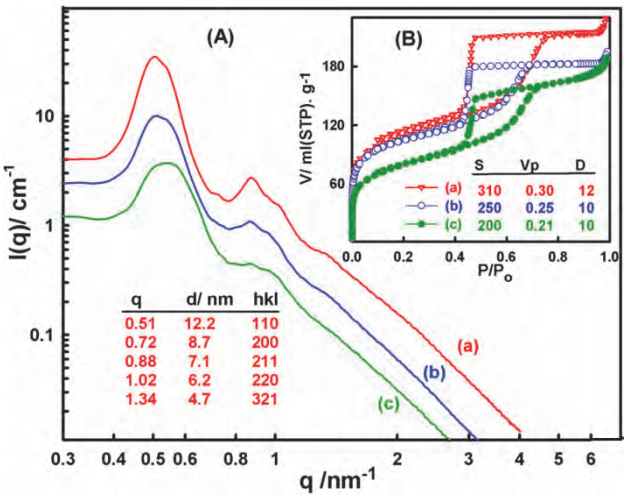

Fig. 11. SAXS (A) and N_2 isotherms (B) of mesofilter membranes based on mesoporous cubic *Im3m* cage silica NT hybrid AAM before (a) and after (b) modification with TMS groups and after removal of the blocked proteins from the AAM surfaces and pores during the second use of the mesofilters (c) (reprinted from El–Safty, 2011).

Nitrogen adsorption/desorption isotherm was used for characterizing the mesoporous materials, including porous silica NTs fabricated inside the AAM pore channels. From the N_2 adsorption isotherm data, various parameters, such as the porous structure, pore size, pore volume and specific surface area, can be estimated. For instance, the mesoporous silica NT membranes have a large surface area (S_{BET}~ 100–310 m^2/g), as shown in Fig. 11(B). The average pore size of HOM silica NTs synthesized using F127 surfactant is about 12 nm. The NTs are stable and retain their mesoporous structures after removal of surfactant, functionalization with the TMS group and use for separation.

FE–SEM images shown in Figs. 12(A)–(B) were recorded with partial etching of the alumina matrix with 8% H_3PO_4 of the silica NT hybrid AAM membrane. SEM micrographs show evidence of the formation of silica NTs inside the 200 nm diameter nanochannels of AAM. After complete etching of the alumina matrix, SEM micrographs reveal that the silica NTs fabricated are well aligned within the AAM pores (Figs. 12 (C)–(D)). Silica NTs with regular and continuous alignment along the perpendicular axis are also observed (Fig. 12(E)) even after the TMS coating inside the pores (Fig. 12(F)). The results, in general, also indicate that the open pore silica NTs fabricated using structure directing surfactants fill the diameter (~200 nm) and most of the length (~60 μm) of the AAM pores (Fig. 12(E)). The NT alignment observed in Fig. 12(F) may have been attained within the inclusive TMS immobilization process inside AAM.

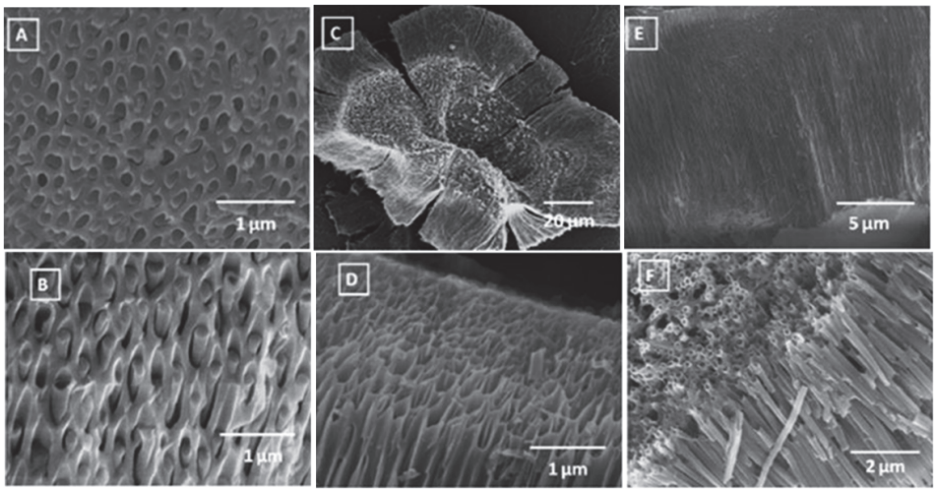

Fig. 12. FE–SEM cross section [(A), (B)] silica NT hybrid AAM membrane after partial etching of the alumina matrix. FE–SEM cross section [(C), (D)] and plan–view (E) images of vertically aligned silica NTs. FE–SEM plan–view image (F) recorded with TMS–silica NTs. (reprinted from El–Safty et al., 2010).

Meanwhile, the HR–TEM images of silica and TMS–silica NTs after the removal of the alumina matrix are shown in Fig. 13. The HR–TEM images clearly reveal large domain sizes of ordered hexagonal mesoporous networks running along the 1D AAM nanochannels. However, the HR–TEM profiles show evidence of the successful formation of hollow mesostructures with a predominantly columnar orientation. The most prominent feature in

the HR–TEM images is the uniform mesoporosity and continuously ordered channels present along all axes of the hexagonal mesoporous silica and TMS–silica NTs that are not significantly distorted under the synthetic conditions. Moreover, the HR–TEM images show evidence that the synthetic route allowed for the controlled formation of free–standing, aligned strands, which permitted a high flux and transport of spherical NPs through the TMS–silica mesopores inside the AAM channels without substantial hindrance. The top–view TEM image shown in Fig. 13(D) indicates variability in the columnar or circular ordering in the AAM channels during the fabrication of silica NTs using this approach.

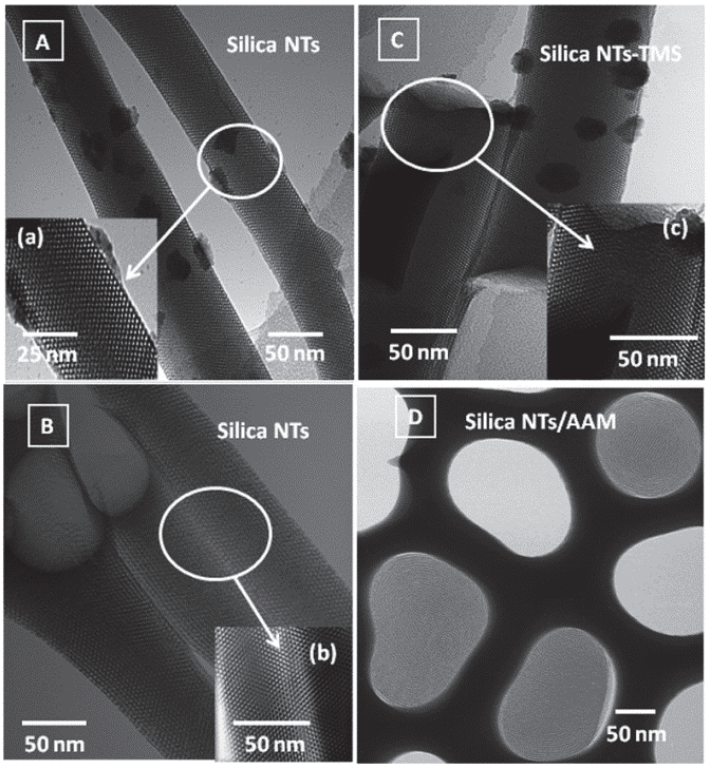

Fig. 13. HR–TEM images of silica [(A), (B)] and TMS–silica (C) NTs after etching of the alumina matrix. (D) TEM image recorded on the top–view of silica NTs hybrid AAM (reprinted from El–Safty et al., 2010)

7. Separation of NPs using HOM silica NTs membranes

The performance of the mesofilter membranes synthesized using a template–guided synthesis for the separation of noble metal NPs, such as Ag, Au, and Pt with different shapes and sizes was evaluated. To synthesize these NPs, two–phase redox reactions were used to control the fabrication of the organic solution–phase Ag NPs with a size distribution ranging from 1 to 16 nm. Initially, 0.081 g of sodium laureate (SL) was dissolved in 5 ml of water. This SL solution was added dropwise to the $AgNO_3$ aqueous solution

($AgNO_3$:0.091 g in 5 ml of water), yielding white precipitates of Ag–SL salt. Collected Ag–SL salt was rinsed with water 10 times and then washed with a small amount of methanol thrice. An organic Ag–SL solution was formed by adding 20 ml of toluene to the methanol (5 ml) solution of Ag–SL salt (0.09 g). Sodium tetrahydroborate solution (Aldrich, 0.0063 g in 10 ml of water) was then added dropwise into the organic Ag–SL solution with vigorous stirring. The toluene phase immediately became yellow. After 10 min of stirring, a yellow toluene phase was collected and stored at 4 °C (Mekawy et al., 2011).

The NPs of gold and platinum were synthesized as well, and the details are presented below. A mixture of 40 mg AuCl, and 1 g oleylamine was dissolved in 10 ml chloroform and stirred for 2h at 60 °C. To this mixture composition, 20 ml acetone was added to precipitate the Au NPs. The precipitated Au NPs were then collected and thoroughly washed with deionized water and ethanol by means of a centrifuge. The Au NPs were dried in air at 45 °C. The synthesis of the PtNPs with octadecylamine followed the same procedures; however, the Pt compound dipotassium hexachloroplatinum (K_2PtCl_6,) was used as the Pt source. The Pt or AuNPs were dispersed in 2 ml of chloroform for subsequent separation.

The schematic design for the size–exclusive separation system of wide distribution sizes of NPs based on TMS–immobilized silica hybrid AAM for producing ultrafine, uniformly–spherical NPs is shown in Fig. 14(A). Typically, the rigid mesoporous silica NTs inside AAM channels having a pore diameter of ~4 nm were used as ultrafine filtration systems (nanofiltration) for separating noble metal NPs fabricated in a wide–range of sizes and spherical/pyramidal morphologies. The grafting of hydrophobic trimethylsilyl (TMS) groups onto the inner pores of the silica NTs walls is very important in creating size– and

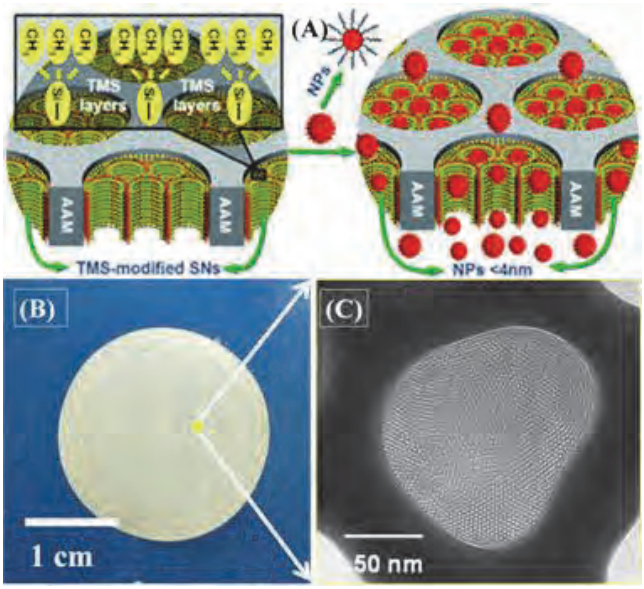

Fig. 14. (A) Schematic design for the size–exclusive separation system, (B) photo of a NT membrane used for NPs separation, and (C) a top–view HRTEM image of a highly ordered porous silica NT.

shape–exclusive separation systems, because the presence of the TMS groups allows the silica NTs to retain their inner pore structure without distortion during the pressurized separation assays that could cause tortuous–pore membranes. Fig.14 shows the size–exclusive porous silica NT membranes, a photo of an NT membrane after calcination (B) and a top–view HRTEM image (C) of a highly ordered porous silica NT used for NP separation.

8. Separation performance of NPs using HOM silica NTs membranes

The separation performance of NPs can be evaluated through quantitative analysis, thus validating the efficiency of the mesoporous TMS–silica hybrid membrane as a size–exclusive separator of NPs. Figs. 15 (A)–(C) show the adsorption spectrum and color change of NPs before and after separation, respectively. As revealed in Fig. 15(A), 20% of the original amount of Ag NPs can be separated in monodispersed and uniform Ag NPs within minutes. However, large NPs with size >4.5 nm are caught in the pores of NTs or on the surface of the hybrid AAM. The color of the membrane changed after the separation process due to the blockage of large NPs, as shown in Fig. 15 (A), inset. The membrane also exhibited effective separation of other NPs, such as gold (Fig. 15(B)) and CdS (Fig. 15(C)). Generally, the amount of blocked NPs depends on the shapes and sizes of NPs in the feed solution. Spherical ones with particles smaller than the pore size of the NT membrane are filtered through the membrane, whereas non–spherical ones with large particles are caught in the pores of NTs or on the surface of the membrane.

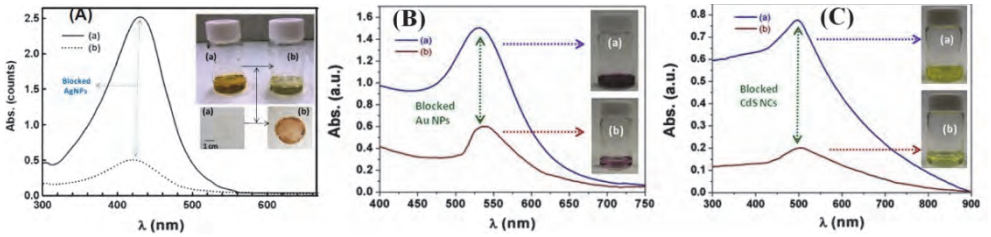

Fig. 15. Adsorption spectrum and color change of NPs before and after separation: (A) Silver NPs; (B) Au NPs; (C) CdS NPs (reprinted from El–Safty et al., 2010, 2011)

Further evaluation of the separation performances of NPs using HRTEM images is shown in Fig. 16. The HRTEM image of Ag NPs before separation (Fig. 16(A)) shows that the NPs are spherical and irregularly–shaped particles with a wide particle size distribution (Fig. 16(D)). After the simple separation process, the TEM analysis shows uniform spherical and regularly shaped particles (Figs. 16(B) and (C)) less than 4.5 nm in diameter, indicating the ultra–fine separation of Ag NPs by size and shape (see the histograms, Figs. 16 (E) and (F)).

The silica NT membrane is not only effective in the separation of Ag NPs, it also performs excellently in the separation of other NPs, including of Au, Pt, CdS, and ZnS. The HR–TEM images of the NPs before filtration show irregularly–shaped NPs with a wide distribution of sizes, as shown in Figs. 17(A), (C), and (E). In contrast, the HR–TEM images taken after filtration, which occurred on a second timescale, show uniformly spherical and regularly–shaped NPs less than 4.5 nm in diameter, indicating the ultra–fine filtration of NPs. Particles size distributions of NPs before and after separation are shown in the insets, respectively.

The size–exclusion cut–off (<4.5 nm) of the membrane filters agrees well with the NLDFT pore–size distribution of the TMS–silica NT. During the filtration process, small-sized particles easily go through the pore channels, whereas the large particles are retained on the surface of membrane. Because the NTs have nanopores with uniform sizes, thus HOM silica NT membranes are effective for the NPs separation. Despite that, after using several times, the particles would stack and block the pore channels, leading to insufficient separation. Therefore, the cleaning processes are required for the reuse of the HOM silica NT membranes. For the cleaning processes, the stacked membranes were settled upside down in the nanofiltration system (Fig. 10). Thereafter, the distilled water and ethanol were filtrated through membrane with the assistance of slight vacuum pumping.

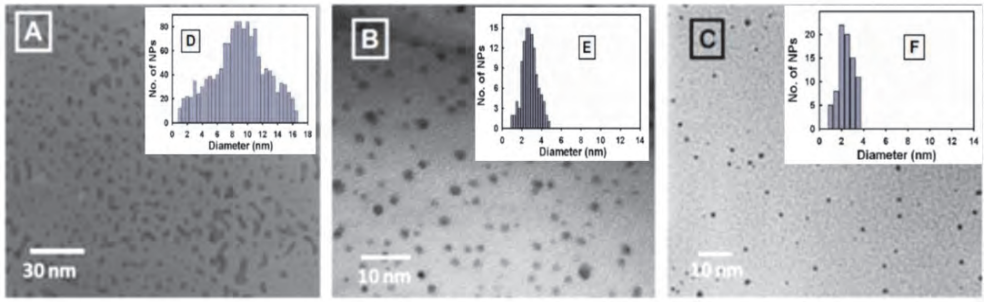

Fig. 16. TEM images of Ag NPs: (A) as–made, (B), (C) after separation through the NT membranes. Insets are correlative particle size distribution (reprinted from Mekawy et al., 2011).

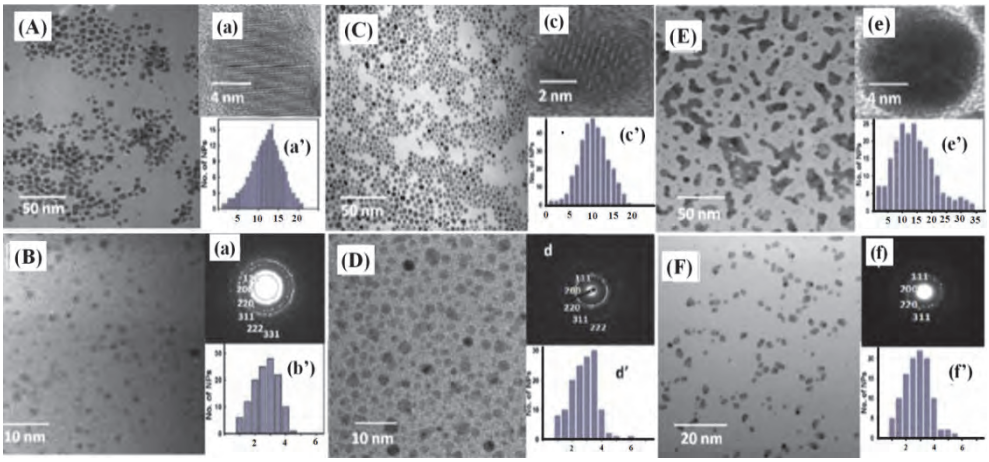

Fig. 17. HR–TEM micrographs of spherical Ag, Au, and Pt NPs before [(A), (C), (E)] and after [(B), (D), (F)] separation using HOM silica NTs membranes. Insets [(A), (C), (E)] are high–magnification TEMs of one NP [(a), (c), (e)] and histogram of NP patterns [(a'), (c'), (e')]. Insets [(B), (D), (F)] are the ED [(b), (d), (f)]and histograms [(b'), (d'), (f')] of Ag, Au, and Pt NPs with fcc phases of cubic *Fm3m* symmetry, respectively (reprinted from El–Safty et al., 2010, 2011)

9. Conclusion and outlook

The development design of hierarchically ordered TMS–silica NTs inside 1D columnar channels has enhanced the potential ability and functionality of the application of membranes in size–exclusive separation systems of particles and small molecules. To design a robust nanofilter, cationic surfactants are used as soft templates for predicting ordered assemblies of surfactant/silica composites through strong interactions within AAM pockets. This approach forms densely–packed NTs in the entirety of the AAM channels. These NTs are coated with layers of organic moieties to create a powerful technique for ultrafine filtration. The nanofilter membranes can then be used effectively to separate several NPs.

The developed membranes are effective in separating novel NPs with particle sizes of less than 4.5 nm. This precise size–cutoff separation is very important in investigating and understanding the quantum size effects in nanomaterials. Physicists have predicted and confirmed that metal NPs in the diameter range of 1–10 nm can display electronic structures, reflecting the electronic band structure of the NPs, as well as exhibit abnormal optical properties. The smaller spherical NPs exhibit a single and sharp localized surface plasmon resonance absorption band in the visible region, while larger spheres exhibit increased scattering and have peaks that broaden significantly and shift towards longer wavelengths. Additionally, the membranes exhibit excellent size–cutoff separation of NPs and help enhance the dispersal of the NPs, with the aggregated NPs becoming mono–dispersed NPs when forced to go through the membrane. The enhancement of dispersal and precise size–cutoff separation of NPs can increase the potential applications of noble metal NPs in biological, optoelectronic and sensing areas, where their optical properties are strongly influenced by interparticle interactions, shapes, and sizes.

Furthermore, multiple strategies are being pursued for the development of nanofilter membranes that fulfill all requirements of high–performance molecular transport and the size–exclusion selectivity of biomolecules and small particles. However, research on the science and engineering of such membranes is needed to combine all of these attributes into practical systems. Advances in nanofabrication methods have opened up exciting new avenues to overcome the limitations of conventional porous materials; however, practical, scalable fabrication processes should also be created. Indeed, there is still a demand for controlled fabrication of mesoscale pores inside metals or metal oxide NTs or NW hybrid AAM. The formation of mesoporous structures inside NTs or NWs can open exciting new applications, including electronics, optics, gas and bio–sensors, and nano–fluidic devices.

10. Acknowledgements

We would like to express our gratitude to the Japan Society for the Promotion of Science (JSPS) for financial support (Grant No. P09606).

11. References

Ahmadi, T.S.; Wang, Z.L.; Green, T.C.; Henglein, A. and El–Sayed, M.A. (1996). Shape–Controlled Synthesis of Colloidal Platinum Nanoparticles, *Science*, Vol. 272, pp. 1924–1925

Asatekin, A. ad Gleason, K.K. (2011). Polymeric nanopore membranes for hydrophobicity based separations by conformal initiated chemical vapor deposition, *Nano Lett.* Vol. 11, pp. 677–686.

Attard, G. S.; Bartlett, P. N.; Coleman, N. R. B.; Elliott, J. M.; Owen, J. R. and Wang, J. H. (1997). Mesoporous Platinum Films from Lyotropic Liquid Crystalline Phases, *Science*, Vol. 278, pp. 838–840.

Bianchini, C. and Shen, P. K. (2009). Palladium–Based Electrocatalysts for Alcohol Oxidation in Half Cells and in Direct Alcohol Fuel Cells, *Chem. Rev.,* Vol. 109, pp. 4183–4206.

Carroll, K. J.; Reveles, J. U.; Shultz, M. D.; Khanna, S. N. and Carpenter, E. E. (2011). Preparation of Elemental Cu and Ni Nanoparticles by the Polyol Method: An Experimental and Theoretical Approach, *J. Phys. Chem. C*, Vol. 115, pp. 2656–2664.

Chen, A. and Holt–Hindle, P. (2010). Platinum–Based Nanostructured Materials: Synthesis, Properties, and Applications, *Chem. Rev.*, Vol. 110, pp. 3767–3804.

Chen, Y.; Gu, X.; Nie, C.G.; Jiang, Z.Y.; Xie, Z.X. and Lin, C. J. (2005). Shape controlled growth of gold nanoparticles by a solution synthesis, *Chem. Commun.*, pp. 4181–4183.

Choi, J.; Jeong, H.K.; Snyder, M.A.; Stoeger, J.A. Masel R.I. and Tsapatsis, M. (2009). Grain boundary defect elimination in a zeolite membrane by rapid thermal processing, *Science*, Vol. 325, pp. 590–593.

Choi, S.H.; Zhang, Y.P.; Gopalan, A.; Lee, K.P. and Kang, H.D. (2005). Preparation of catalytically efficient precious metallic colloids by γ–irradiation and characterization, *Colloids Surf. A*, Vol. 256, pp. 165–170.

Cott, D. J.; Petkov, N.; Morris, M. A.; Platschek, B.; Bein, T. and Holmes, J. D. (2006). Preparation of oriented mesoporous carbon nano–filaments within the pores of anodic alumina membranes, *J. Am. Chem. Soc.*, Vol. 128, pp. 3920–3921.

Dong, X.; Ji, X.; Jing, J.; Li, M.; Li, J. and Yang, W. (2010). Synthesis of Triangular Silver Nanoprisms by Stepwise Reduction of Sodium Borohydride and Trisodium Citrate, *J. Phys. Chem. C*, Vol. 114, pp. 2070–2074.

El–Safty, S.A.; Mekawy, M.; Yamaguchi, A.; Shahat, A.; Ogawa, K. and Teramae, N. (2010). Organic–inorganic mesoporous silica nanostrands for ultrafine filtration of spherical nanoparticles, *Chem. Commun.*, Vol. 46, pp. 3917–3919.

El–Safty, S.A.; Shahat, A.; Mekawy, M. Hoa, N. Warkocki, W. and Ohnuma, M. (2010). Mesoporous silica nanotubes hybrid membranes for functional nanofiltration, *Nanotechnology*, Vol. 21, 375603.

El–Safty, S.A.; Shahat, A.; Awual, Md. R. and Mekawy, M. (2011). Large three–dimensional mesocage pores tailoring silica nanotubes as membrane filters: nanofiltration and permeation flux of proteins, *J. Mater. Chem.*, Vol. 21, pp. 5593–5603.

El–Safty, S.A.; Shahat, A.; Warkocki, W. and Ohnuma, M. (2011). Building–Block–Based Mosaic Cage Silica Nanotubes for Molecular Transport and Separation, *Small*, Vol. 7, pp. 62–65.

El–Safty, S.A. (2011). Designs for Size–Exclusion Separation of Macromolecules by Densely Engineered Mesofilters, *Trends Anal. Chem*., Vol. 30, 447–458.

El–Safty, S.A. and Shenashen, M.A. (2011). Size–selective separations of biological macromolecules on mesocylinder silica arrays, *Anal. Chim. Act*., pp.151–161.

Enders, D.; Nagao, T.; Pucci, A.; Nakayama, T. and Aonoa, M. (2011). Surface-enhanced ATR-IR spectroscopy with interface-grown plasmonic gold-island films near the percolation threshold, *Phys. Chem. Chem. Phys.*,Vol. 13, pp. 4935–4941.

Faraday, M. (1857). The Bakerian lecture: experimental relations of gold (and other metals) to light, *Philos.Trans.R.Soc.London*, Vol. 147, 145.

Fukuoka, A.; Araki, H.; Sakamoto, Y.; Sugimoto, N.; Tsukada, H.; Kumai, Y.; Akimoto, Y. and Ichikawa, M. (2002). Template Synthesis of Nanoparticle Arrays of Gold and Platinum in Mesoporous Silica Films, *Nano Letters*, Vol. 2, pp. 793–795.

Gin D.L. and Noble, R.D. (2011). Designing the next generation of chemical separation membranes, *Science*, Vol. 332, pp. 674–676.

Gong, Z.; Ji, G.; Zheng, M.; Chang, X.; Dai, W.; Pan, L.; Shi, Y. and Zheng, Y. (2009). Structural Characterization of Mesoporous Silica Nanofibers Synthesized Within Porous Alumina Membranes, *Nanoscale Res. Lett.*, 2009, 4, 1257–1262.

Green, M. and O'Brien, P. (2000). A simple one phase preparation of organically capped gold nanocrystals, *Chem. Commun*., pp. 183–184.

Grzelczak, M.; Pérez–Juste, J.; Mulvaney P. and Liz–Marzán, L. M. (2008). Shape control in gold nanoparticle synthesis, *Chem. Soc. Rev*., Vol. 37, pp. 1783–1791.

Han, J.Y.; Fu, J. P. and Schoch, R. B. (2008). Molecular sieving using nanofilters: Past, present and future. *Lab. Chip*, Vol. 8, pp. 23–33.

Hashim, N. A.; Liu, Y. and Li, K. (2011). Preparation of PVDF hollow fiber membranes using SiO_2 particles: The effect of acid and alkali treatment on the membrane performances, *Ind. Eng. Chem. Res*., Vol. 50, pp. 3035–3040.

He, X.; Lie, J.A.; Sheridan, E. and Hagg, M.B. (2011). Preparation and Characterization of Hollow Fiber Carbon Membranes from Cellulose Acetate Precursors, *Ind. Eng. Chem. Res.* Vol. 50, pp. 2080–2087.

Henglein, A. (1998). Colloidal Silver Nanoparticles: Photochemical Preparation and Interaction with O_2, CCl_4, and Some Metal Ions, *Chem. Mater*., Vol. 10, pp. 444–450.

Herricks, T.; Chen, J. and Xia, Y. (2004). Polyol synthesis of platinum nanoparticles: control of morphology with sodium nitrate, *Nano Lett*., Vol. 4, pp. 2367–2371.

Hoa, N.D and El–Safty, S.A. (2011). Highly sensitive and selective volatile organic compound gas sensors based on mesoporous nanocomposite monoliths, *Anal. Methods*, Vol. 3, pp. 1948–1956.

Hoa, N.D and El–Safty, S.A. (2011). Gas nanosensor design packages based on tungsten oxide: mesocages, hollow spheres, and nanowires, *Nanotechnology* Vol. 22, pp. 485503.

Hoa, N.D and El–Safty, S.A. (2011), Meso- and Macroporous Co_3O_4 Nanorods for Effective VOC Gas Sensors, *J. Phys. Chem. C*, Vol.115, pp 8466–8474.

Hoa, N.D and El–Safty, S.A. (2011). Synthesis of Mesoporous NiO Nanosheets for the Detection of Toxic NO_2 Gas, *Chem. Eur. J*. Vol. 17, pp. 12896 – 12901.

Horswell, S.L.; Kiely, C.J.; O'Neil, I.A. and Schiffrin, D.J. (1999). Alkyl Isocyanide–Derivatized Platinum Nanoparticles, *J. Am. Chem. Soc.*, Vol. 121, p. 5573

Horinouchi, S.; Yamanoi, Y.; Yonezawa, T.; Mouri, T. and Nishihara, H. (2006). Hydrogen Storage Properties of Isocyanide–Stabilized Palladium Nanoparticles, *Langmuir*, Vol. 22 (4), pp. 1880–1884.

Hill, J. J.; Cotton, S.P. and Ziegler, K.J. (2009). Alignment and Morphology Control of Ordered Mesoporous Silicas in Anodic Aluminum Oxide Channels by Electrophoretic Deposition, *Chem. Mater.*, Vol. 21, pp. 1841–1846.

Hieda, J.; Saito, N.; Takai, O. (2008). Exotic shapes of gold nanoparticles synthesized using plasma in aqueous solution, *J. Vac. Sci. Technol. A,* Vol. 26, pp. 854–856

Hsieh, H.P. (1991). Inorganic membrane reactors, *Catal. Rev. Sci. Eng*. Vol. 33, pp. 1–70.

Iglesias, R.A.; Tsow, F.; Wang, R.; Forzani, E. S. and Tao, N. (2009). Hybrid separation and detection device for analysis of benzene, toluene, ethylbenzene, and xylenes in complex samples, *Anal. Chem.*, Vol. 81, pp. 8930–8935.

Jang, K.S.; Kim, H.J.; Johnson, J.R.; Kim, W.; Koros, W.J.; Jones, C.W. and Nair, S. (2011). Modified mesoporous dilica gas separation membraneson polymeric hollow fibers, *Chem. Mater.* Vol. 23, pp. 3025–3028.

Jones, M. R.; Osberg, K. D.; Macfarlane, R. J.; Langille, M. R. and Mirkin, C. A. (2011). Templated Techniques for the Synthesis and Assembly of Plasmonic Nanostructures, *Chem. Rev*. Vol. 111, pp. 3736–3827.

Kim, F.; Connor, S.; Song, H.; Kuykendall, T. and Yang, P. (2004). Platonic Gold Nanocrystals, *Angew. Chem., Int. Ed.*, Vol. 43, pp. 3677–3682.

Kim, S.W.; Park, J.; Jang, Y.; Chung, Y.; Hwang, S.; Hyeon, T. and Kim, Y.W. (2003). Synthesis of Monodisperse Palladium Nanoparticles, *Nano Letters,* Vol. 3, pp. 1289–1291.

Kosmala, A.; Wright, R.; Zhang, Q. and Kirby, P. (2011). Synthesis of silver nano particles and fabrication of aqueous Ag inks for inkjet printing, *Mat. Chem. Phys.* Vol. 129, pp. 1075–1080.

Kurihara, L. K.; Chow, G. M. and Schoen, P. E. (1995). Nanocrystalline metallic powders and films produced by the polyol method, *Nano. Mat.*, Vol. 5, pp. 607–613.

Lee, K.J.; Min, S. H. and Jang, J. (2008), (2009). Vapor–Phase Synthesis of Mesostructured Silica Nanofibers Inside Porous Alumina Membranes, *Small*, Vol. 4, pp. 1945–1949. (b) Mesoporous Nanofibers from Dual Structure–Directing Agents in AAO: Mesostructural Control and their Catalytic Applications, *Chem. Eur. J.* Vol. 15, 2491–2495.

Lim, B.; Lu, X.; Jiang, M.; Camargo, P.H.C.; Cho, E.C.; Lee, E.P. and Xia, Y. (2008). Facile synthesis of highly faceted multioctahedral Pt nanocrystals through controlled overgrowth, *Nano Lett.*, Vol. 8, pp. 4043–4047.

Liu, Z.; Zu, Y.; Fu, Y.; Meng, R.; Guo, S.; Xing, Z. and Tan, S. (2010. Hydrothermal synthesis of histidine–functionalized single–crystalline gold nanoparticles and their pH–dependent UV absorption characteristic, *Coll. Surfaces B.*, Vol. 76, pp. 311–316.

Liz–Marzán, L.M. (2004). Nanometals: formation and color, *Mater. Today*, pp. 26–31.

Mekawy, M.; Yamaguchi, A.; El–Safty, S.A.; Itoh, T. and Teramae N. (2011). Mesoporous Silica Hybrid Membranes for Precise Size–Exclusive Separation of Silver Nanoparticles" *J. Colloid Interface Sci.* Vol. 355, pp. 348–358.

Miyazaki, A.; Balint, I. and Nakano, Y. (2003). Morphology Control of Platinum Nanoparticles and their Catalytic Properties, *J. Nano. Res*. Vol. 5, p. 69

Moses, J.; Khn, R.; Dblinger, M. and Bein, T. (2010). Electrodeposition of Copper and Silver Nanowires in Hierarchical Mesoporous Silica/Anodic Alumina Nanostructures, *Chem. Mater*., Vol. 22, pp. 5430–5436.

Nakamura H. and Matsui, Y. (1995). Silica Gel Nanotubes Obtained by the Sol–Gel *J. Am. Chem. Soc.*, Vol. 117, pp. 2651– 2652.

Nath, N. and Chilkoti, A. (2002). A Colorimetric Gold Nanoparticle Sensor To Interrogate Biomolecular Interactions in Real Time on a Surface, *Anal. Chem.* Vol. 74, pp. 504-509.

Nemamcha, A.; Rehspringer, J.L. and Khatmi, D. (2006). Synthesis of Palladium Nanoparticles by Sonochemical Reduction of Palladium(II) Nitrate in Aqueous Solution, *J. Phys. Chem. B,* Vol. 110, pp. 383–387.

Nieto, J.T.; Arvalo, A. and Garca, J.J. (2008). Catalytic Desulfurization of Dibenzothiophene with Palladium Nanoparticles, *Inorg. Chem*., Vol. 47, pp. 11429–11434.

Niu, W.; Zhang, L. and Xu, G. (2010). Shape–Controlled Synthesis of Single–Crystalline Palladium Nanocrystals, *ACS Nano,* Vol. 4, pp. 1987–1996.

Onizawa, S.; Aoshiba, K.; Kajita, M.; Miyamoto, Y. and Nagai, A. (2009). Platinum nanoparticle antioxidants inhibit pulmonary inflammation in mice exposed to cigarette smoke, *Pulm. Pharmacol. Ther.* Vol. 22(4), pp. 340–349.

Pal, A.; Shah, S. and Devi, S. (2007). Synthesis of Au, Ag and Au–Ag alloy nanoparticles in aqueous polymer solution, *Colloids Surf. A*, Vol. 302, pp. 51–57.

Petroski, J.M.; Wang, Z.L.; Green, T.C. and El–Sayed, M.A. (1998). Kinetically controlled growth and shape formation mechanism of platinum nanoparticles, *J. Phys. Chem. B*, Vol. 102, pp. 3316–3320.

Platschek, B.; Petkov, N.; Himsl, D.; Zimdars, S.; Li, Z.; Khn, R. and Bein, T. (2008). Vertical Columnar Block–Copolymer–Templated Mesoporous Silica via Confined Phase Transformation, *J. Am. Chem. Soc.*, Vol. 130, pp. 17362–17371.

Polte, J.; Ahner, T.T.; Delissen, F.; Sokolov, S.; Emmerling, F.; Thnemann, A. F. and Kraehnert, R. (2010). Mechanism of Gold Nanoparticle Formation in the Classical Citrate Synthesis Method Derived from Coupled In Situ XANES and SAXS Evaluation, *J. Am. Chem. Soc.*, Vol. 132 (4), pp. 1296–1301.

Robeson, L. M. (2008). The upper bound revisited, *J. Membr. Sci.* Vol., 320, 390–400.

Roy, P.S.; Bagchi, J. and Bhattacharya, S. K. (2009). Size–controlled synthesis and characterization of polyvinyl alcohol coated palladium nanoparticles, *Transition Met. Chem.,* Vol. 34, pp. 447–453.

Salkar, R. A.; Jeevanandam, P.; Aruna, S. T.; Koltypin, Y. and Gedanken, A. (1999).The sonochemical preparation of amorphous silver nanoparticles *J. Mater. Chem.*, Vol. 9, pp. 1333–1335.

Santos, I. P. and Liz–Marzán, L.M. (2002). Synthesis of Silver Nanoprisms in DMF, *Nano Lett.*, Vol. 2, pp. 903–905.

Shen, J.; Shi, M.; Yan, B.; Ma, H.; Li, N. and Ye, M. (2011). One–pot hydrothermal synthesis of Ag–reduced graphene oxide composite with ionic liquid, *J. Mater. Chem.*, Vol. 21, pp.7795–7801.

Shrivastava, S.; Bera, T.; Singh, S. K.; Singh, G.; Ramachandrarao, P. and Dash, D. (2009). Characterization of Antiplatelet Properties of Silver Nanoparticles, *ACS Nano*, Vol. 3, pp.1357–1364

Siekkinen, A. R.; McLellan, J. M.; Chen, J. and Xia, Y. (2006). Rapid synthesis of small silver nanocubes by mediating polyol reduction with a trace amount of sodium sulfide or sodium hydrosulfide, *Chem Phys Lett.* Vol. 432, pp. 491–496.

Soria, R. (1995). Overview on industrial membranes, *Catal. Today*, Vol. 25, pp. 285–290.

Tian, N.; Zhou, Z.Y.; Sun, S.G.; Ding, Y. and Wang, Z.L. (2007). Synthesis of Tetrahexahedral Platinum Nanocrystals with High–Index Facets and High Electro–Oxidation Activity, *Science*, Vol. 316, pp. 732–735.

Tsung, C.K.; Kuhn, J.N.; Huang, W.; Aliaga, C.; Hung, L.; Somorjai, G. A. and Yang, P. (2009). Sub–10 nm Platinum Nanocrystals with Size and Shape Control: Catalytic Study for Ethylene and Pyrrole Hydrogenation, *J. Am. Chem. Soc.*, Vol. 131, pp. 5816–5822.

Ulbricht, M. (2006). Advanced functional polymer membranes, *Polymer,* Vol. 47, pp. 2217–2262.

V. Amendola, S. Polizzi, and M. Meneghetti, Free Silver Nanoparticles Synthesized by Laser Ablation in Organic Solvents and Their Easy Functionalization, *Langmuir,* 2007, 23, 6766–6770

Wagner, J. (2001). Practical tips and hints, in: Membrane Filtration Handbook, Chemical Engineering, 2nd Edn, 2001

Walker, C. H.; John, J.V.St. and Neilson, P.W. (2001). Synthesis and Size Control of Gold Nanoparticles Stabilized by Poly(methylphenylphosphazene), *J. Am. Chem. Soc.*, Vol. 123, pp. 3846–3847.

Welch, C. M. and Compton, R.G. (2006). The use of nanoparticles in electroanalysis: a review, *Anal. Bioanal. Chem.* , Vol. 384, pp. 601–619.

Willets, K. A. and Duyne, R. P. V. (2007). Localized Surface Plasmon Resonance Spectroscopy and Sensing, *Annu. Rev. Phys. Chem.* Vol. 58, pp. 267–297.

Wu, Y. ; Livneh, T.; Zhang, Y. X.; Cheng, G.; Wang, J.; Tang, J.; Moskovits, M. and Stucky G.D. (2004). Templated Synthesis of Highly Ordered Mesostructured Nanowires and Nanowire Arrays, *Nano Lett.*, Vol. 4, pp. 2337–2342.

Xiao, J. and Qi, L. (2011). Surfactant–assisted, shape–controlled synthesis of gold nanocrystals, *Nanoscale*, Vol. 3, pp. 1383–1396.

Xia, Y.; Xiong, Y.; Lim, B. and Skrabalak, S.E. (2009). Shape–Controlled Synthesis of Metal Nanocrystals: Simple Chemistry Meets Complex Physics?, *Angew. Chem. Int. Ed.,* Vol. 48, pp. 60–103.

Yang, Y.; Matsubara, S.; Xiong, L.; Hayakawa, T. and Nogami, M. (2007). Solvothermal Synthesis of Multiple Shapes of Silver Nanoparticles and Their SERS Properties, *J. Phys. Chem. C*, Vol. 111, pp. 9095–9104.

Xiong, Y.; Chen, J.; Wiley, B.; Xia, Y.; Aloni, S. and Yin, Y. (2005). Understanding the Role of Oxidative Etching in the Polyol Synthesis of Pd Nanoparticles with Uniform Shape and Size, *J. Am. Chem. Soc.*, Vol. 127, pp. 7332–7333.

Yoo, S.; Ford, D. M. and Shantz, D. F. (2006). Synthesis and characterization of uniform alumina–mesoporous silica hybrid membranes, *Langmuir, Vol. 22, pp.* 1839–1845.